Title:

GPR161 anchoring of PKA consolidates GPCR and cAMP signaling

Running title: **GPR161 is a type I AKAP**

Verena A Bachmann[1], Johanna E Mayrhofer[1], Ronit Ilouz[2], Ruth Röck[1], Philipp M Tschaikner[3], Philipp Raffeiner[1], Mathieu Courcelles[4,5], Tsan-Wen Lu[2], George S Baillie[6], Pia Aanstad[3], Ulrich Stelzl[7], Susan S Taylor[2], Eduard Stefan[1]

[1] Institute of Biochemistry and Center for Molecular Biosciences, University of Innsbruck, Innrain 80/82, 6020 Innsbruck, Austria
[2] Department of Pharmacology and Department of Chemistry and Biochemistry University of California, San Diego, California 92093, United States
[3] Institute of Molecular Biology, University of Innsbruck, Technikerstrasse 25, 6020 Innsbruck, Austria
[4] Institute for Research in Immunology and Cancer, Université de Montréal, H3C 3J7 Montréal, Québec, Canada
[5] Département de Biochimie, Université de Montréal, H3C 3J7 Montréal, Québec, Canada
[6] Institute of Cardiovascular and Medical sciences, CMVLS, University of Glasgow, Glasgow, G128QQ, UK.
[7] Max Planck Institute for Molecular Genetics (MPIMG), Otto-Warburg Laboratory, Ihnestraße 63-73, 14195 Berlin, Germany

Write to Pierre Thibault[3] & Stephen W Michnick[4]

Correspondence should be addressed to Eduard Stefan (eduard.stefan@uibk.ac.at)

Abstract.

Scaffolding proteins organize the information flow from activated G protein-coupled receptors (GPCRs) to intracellular effector cascades spatially and temporally. By this means signaling scaffolds such as A-kinase anchoring proteins (AKAPs) compartmentalize kinase activities and ensure substrate selectivity. Using a phospho-proteomics approach we identified a physical and functional connection between protein kinase A (PKA) and GPR161 signaling. We show that the orphan GPCR GPR161 on its own contains the structural features to function as high-affinity type I AKAP. Binary complex formation affects plasma membrane targeting in cells and provokes GPR161-mediated PKA recruitment into the primary cilium of zebra fish embryos. We illustrate that receptor-anchored PKA complexes enhance cAMP-mediated GPR161 phosphorylation, which is regarded as one general principal for regulating GPCR desensitization. In addition, we unveiled that distinct disease mutations of PKA regulatory subunits differentially contribute to spatially restricted interactions of GPR161-anchored PKA type I holoenzyme complexes. Thus, the integrity of the membrane-targeted and cAMP-sensing GPR161:PKA signalosome needs to be considered in analyzing, interpreting, and pharmaceutical targeting of GPR161-involved and PKA-associated human diseases.

Introduction

Scaffolding proteins act as flexible organizing centers to consolidate and propagate the cellular information flow from activated cell-surface receptors to intracellular effector cascades. Activated G protein-coupled receptors (GPCRs) engage pleiotropic scaffolds such as beta-arrestin and A-kinase anchoring proteins (AKAPs) to recruit cytoplasmic downstream effector molecules[1-5]. Thus compartmentalized GTPases, kinases and phosphatases act as GPCR-linked molecular switches to spatially and temporally control signal propagation. In the classical view of GPCR signaling, extracellular ligands bind to the receptor which catalyzes the intracellular GDP/GTP exchange and activation of receptor-associated trimeric G protein (α:β:γ) combinations[3]. In addition to receptor dimerization, GPCR signaling and trafficking involve G protein-dependent and G protein-independent intracellular interactions with scaffolds such as beta-arrestin and AKAPs[1, 2, 6, 7]. Receptor-interacting proteins and kinase activities contribute to the fine-tuning of GPCR localization and activities[5, 8-10]. Different AKAPs coordinate and compartmentalize diffusible second messenger responses through anchoring of cAMP-dependent type I or type II protein kinase A (PKA) holoenzymes, composed of two regulatory (RIα/β or RIIα/β) and two catalytic (PKAc) subunits, to discrete subcellular localizations[11]. The four R subunits have different expression patterns and are functionally non-redundant. The growing family of AKAPs are functionally diverse; however, all AKAPs contain an amphipathic helix, which account for nano-molar binding affinities to PKA R subunit dimers[12, 13]. Moreover, it has been shown that additional components of the cAMP signaling machinery physically interact with AKAPs, such as GPCRs, adenylyl cyclases (ACs) and phosphodiesterases (PDEs)[1, 6, 14-16]. Deregulation of the GPCR-cAMP-PKA pathways contribute to a variety of human diseases. Mutations in different PKA subunits manipulate PKA dynamics and activities and contribute to specific disease patterns. Mutations activating cAMP/PKA signaling contribute e.g. to carcinogenesis or degenerative diseases, while inactivating mutations cause e.g. hormone resistance[17-27]. Therefore, revealing the composition of signaling complexes formed upon GPCR and kinase activation is critical for understanding the modes of kinase activation. In-depth analyses of transient protein:protein interactions (PPIs) along with the phosphorylation dynamics have the potential to reveal conditional signal flow and thus may help to explain

pathological implications of second-messenger signaling. Such a strategy will lead to a better understanding of cAMP-signaling, which boosts proliferation in many cell types but inhibits cell growth in others[28-31]. Using a proteomics approach we have identified a physical and functional interaction of an orphan GPCR with distinct PKA subunits. We demonstrate that GPR161 is both a type I AKAP and a PKA substrate.

Results.

Protein:protein interaction (PPI) information is typically generated in exogenous systems such as the yeast two-hybrid approaches or from affinity purification followed by mass spectrometry of overexpressed tagged proteins[32]. Here, we affinity-purified endogenous PKA complexes from the osteosarcoma cell line U2OS after simulation of chronic stress conditions by selective activation of β_2AR; a GPCR linked to cAMP-mobilization and PKA activation[10]. We applied PKA-selective Rp-8-AHA-cAMP-agarose resin to isolate endogenous PKA complexes under varying ligand occupancies and timings of cAMP-generating ACs and endogenous β_2AR from U2OS cells. Following proteomic and phospho-proteomic analyses (liquid chromatography - mass spectrometry), we generated an integrated PKA PPI network representing a consistent set of PKA associated proteins linked to PKA signaling: We confirmed the enrichment of all four PKA regulatory subunits (RIα, RIβ, RIIα, RIIβ) and two PKA catalytic subunits (PKAcα/β). We organized the interaction partners in a fan-shaped pattern surrounding the centered PKA subunits providing a combined overview of 92 affinity-purified proteins using Rp-8-AHA-cAMP-resin (**Supplementary Fig. 1&2; Supplementary Table 1; Supplementary information**). However, to ease the selection of functionally linked PKA interactors we mapped all the detected phosphorylation sites and present co-purified phospho-proteins with their identified sites in a PKA centric illustration including 76 known phosphorylation and 33 potential PKA group phosphorylation sites (**Fig. 1a**). With the Rp-8-AHA-cAMP bound PKA subunits we co-precipitated the AKAPs 1,2,3,5,8,9&11, which are known binary interaction partners of R subunits, along with further components of the cAMP machinery (PDE4A, PDE4IP) and kinase signaling. We discovered that these AKAP-organized PKA complexes contain additional proteins involved in protein transport, RNA binding and discrete posttranslational modifications (*e.g.* HDAC6 and PRMT6). Our

analyses identified a large set of proteins attributed to metabolic signaling, thus underlining established and revealing novel connections of PKA to metabolic pathways. Interestingly, also not easy accessible interactors like membrane receptors and channels (*e.g.* GPR161, ADORA3 and TRPC3, KCNJ3) were identified in the macromolecular PKA complex. This observation prompted us to characterize an unforeseen physical link to a membrane protein, the orphan GPCR GPR161, which actually contains a canonical PKA phosphorylation consensus site in its carboxy-terminus (CT, ...^{427}RRSS^{430}…). This decision was endorsed by previous studies and observations: First, it has been previously shown that the GPR161-CT is critically implicated in developmental processes (lens development, neurulation) through implications in GPR161 localization (**Fig. 1b**)[33]. Second, both GPR161 and PKA activities are involved in hedgehog signaling in the primary cilium (**Fig. 1b**)[34, 35]. Third, a physical connection of PKAc with GPR161 has been proposed in a recent network study using tagged PKA subunits as bait[36]. Fourth, upregulated GPR161 expression patterns have been found in triple negative breast cancer[37]. This begs the questions how physical PKA associations with this orphan receptor (indirect or direct?) might contribute to GPR161 functions.

To facilitate the analyses of the function of the cytoplasmic localized GPR161-CT (=*CT*$^{342\text{-}529}$), we generated different glutathione-sepharose-transferase (GST) expression constructs to investigate complex formation with PKA. In GST pulldown assays we precipitated endogenous PKA subunits from HEK293 cell lysates with GST- *CT*$^{342\text{-}529}$. We significantly enriched endogenous RI:PKAc complexes. No binding of RIIβ was detectable. Addition of excess of cAMP to the precipitation reaction initiated PKA complex dissociation. In contrast to diminished PKAc binding, the GST-*CT*$^{342\text{-}529}$:RI complex was insensitive to cAMP-binding (**Fig. 1c**). These data underline that binding of PKAc to GPR161 is mediated through RI subunits. To determine specific amino acids in GPR161 that are responsible for RIα binding we performed a peptide spotting experiment. We spotted overlapping 25-mer peptides derived from GPR161-*CT*$^{342\text{-}529}$ sequence onto a membrane and overlaid it with recombinant RIα-*his*^{6} (hexa-histidine tagged), as previously described[38]. In the GPR161-CT we identified one possible binding site for RIα with the core region …LDSYAASLAKAIE… (**Fig. 1d**). This sequence stretch is part of an amphipathic helix with the centered Leu465 (**Fig. 1e**) which we substituted in the next

experiments for proline. With different recombinant GST-CT variants of GPR161 we repeated the pulldown experiments with recombinant RIα *in vitro*. We confirmed the binary interaction of RIα with wild type GPR161-$CT^{342-529}$, and once again this complex is insensitive to cAMP binding to RIα. All shorter variants of GPR161-CT which contain the core LAKAIE motif showed interaction with recombinant RIα. The GST-$CT^{342-529}$ mutant containing the L465P substitution showed no binding to RIα (**Fig. 2a**). These experiments confirmed a binary PPI, GPR161-CT:RIα, *in vitro*. Moreover, it proved that an amphipathic helix in the GPCR-CT directly mediates PPI with type I PKA R subunits as it has been described in detail for all other members of the AKAP family.

We next repeated the experiment with cell lysates. We observed a similar pattern of PPI with RIα. Endogenous RIIβ did not bind to any of the GST-fused CTs (**Supplementary Fig. 3a**). With overexpressed GPR161 variants we repeated cAMP-precipitation experiments as performed for Fig. 1a and Supplementary Figs.1&2. We show that cAMP-bound R subunits are sufficient for the precipitation of full-length GPR161 tagged with Venus YFP. In comparison, the GPT161-ΔCT mutant (L465P) showed no PPI (**Supplementary Fig. 3b**). This data confirms our peptide array experiments and demonstrates that the CT mediates binary PPI with RIα PKA subunits in cells.

Next we tagged the $CT^{378-529}$ N- and C-terminally with hexa-histidine tags (his^6) to increase its solubility. In contrast to the $CT^{378-529}$L465P mutant, sole expression of the wild type fusion protein in bacteria showed low solubility. However, following bacterial co-expression of $CT^{378-529}$ and untagged RIα we observed enhanced solubility of the $CT^{378-529}$. Strikingly, in affinity purifications using Ni-NTA resin we co-purified significant amounts of untagged RIα with $CT^{378-529}$; we observed no PPI with the L465P mutant CT of GPR161 (**Fig. 2b**). A subsequent cAMP-precipitation showed the stability and specificity of this binary PPI *in vitro* (**Supplementary Fig. 4**). The significant enrichment of RIα with his^6-$CT^{378-529}his^6$ suggests that a ratio of CT:RIα complexes of 1:2 is favored. This would underline the AKAP concept describing that one R subunit dimer interacts with the GPR161-AKAP helix. In dot blot analyses we compared binding of recombinant RIα to amphipathic helices of selected AKAPs[39]. We observed that binding of RI also depends on the length and on the positioning of critical amino acids of the selected amphipathic helices. In this *in vitro* assay we confirmed specific binding of RIα to sequences

surrounding the LAKAIE motif; binding was abolished with peptides containing proline substitutions (**Supplementary Fig. 5**). To understand the specificity of GPR161-CT binding we analyzed the helical propensity of GPCR161-CT with Agadir, an algorithm that predicts the helical content of peptides[40]. The α-helix is predicted to span from D459 to L477. The modified L465 is located in the middle of the helix (**Supplementary Fig. 6a**). In structure-based alignments of GPR161 with RI specific AKAPs and dual specific AKAPs we identified residues that are similar and bind the D/D domain hydrophobic groove (shown in red; **Fig. 2c**). RII specific AKAPs do not align the same way (**Supplementary Fig. 6b**). We present a structural model of RIα-D/D domain in complex with GPR161 (457-479), based on RIα-D/D domain in complex with D-AKAP2[13]. There are four conserved binding pockets in the D/D domain, each allowing two hydrophobic residues of the AKAP amphipathic helix to dock onto the hydrophobic groove (**Fig. 2d**). These hydrophobic residues are conserved in RI specific AKAPs (shown as surfaces in Fig. 2d). All other GPR161 specific residues, within the predicted helix, which do not align with other RI specific AKAPs and are solvent exposed (shown in cyan). Next, we subjected the corresponding peptide $CT^{459-477}$ to fluorescence polarization measurements with full length RIα or RIIβ. We observed selective and high affinity binding of the peptide to RIα with a Kd of 6.039 nM (±0.105). With RIIβ homodimer we observed no binding (**Fig. 2e**). This is in agreement with the pulldown assays illustrated in Fig.1c und Supplementary Fig. 3a showing exclusive RI binding to the different CTs. Assessments of AKAP sequences and the structural model with previously published RIα and RIIα structures explains the selectivity for GPR161-CT binding to RIα[13, 41]: The structure comparison of the D/D domains of RIα and RIIα unveils a more extended hydrophobic surface at the N-terminus of RIα that includes a third helix (α0-Helix) instead of a short strand that is a conserved feature of RII subunits. Embedded within these RI-specific pockets are the disulfide bonds that are also a unique feature of RI D/D domains. $Cys16^A$ in the α0-Helix forms a disulfide bond with $Cys36^B$. The disulfide bond stabilizes the N-terminus of the RI-subunits potentially allowing them to serve as redox sensor. In contrast, the RII subunits have only 2 helices and no extra α0-Helix or cysteines in their D/D domains[13]. We also highlight in the sequence alignment shown in Fig. 2c s that the N and C terminus of the amphipathic helix of GPR161 provide additionally unique hydrophobic interactions. The red underlayed

Leucins of the GPR161 AKAP motif bury the RIα D/D domain disulfide bonds thereby creating two additional pockets, one at each end. These two hydrophobic residues explain the preference of GPR161 for RI binding. These Leucines not only provide additional binding surfaces to the RIα D/D domain but would also protect the RIα disulfide bonds (Cys16-37) from the redox environment (**Fig. 2f**).

To investigate the function of PKA:GPR161 interaction we analyzed the dynamics of receptor localization and phosphorylation. **Fig. 3a** depicts sequence elements in the GPR161-CT which we analyzed. As starting point we constructed mammalian expression vectors of different GPR161-variants tagged with Venus-YFP at the carboxy-terminus. We tested the consequence of general and GPCR-mediated cAMP-elevation on GPR161 phosphorylation. We transiently overexpressed Venus-YFP tagged wild type receptor along with the S429A/S430A and L465P mutants in HEK293 cells stably expressing β_2 adrenergic receptors (β_2AR). β_2AR are coupled to the stimulatory G protein α_s ($G\alpha_s$) and therefore are linked to cAMP elevation. We elevated cellular cAMP-levels with Forskolin and/or the βAR ligand Isoproterenol. Following immunoprecipitation of the GPR161 variants we tracked changes of the phosphorylation status of GPR161 variants with a general PKA substrate antibody. In contrast to the L465P mutant we showed that the overexpressed wild type and S429A/S430A receptor bind endogenous RI. Upon cAMP-elevations we observed a significant elevation of GPR161 phosphorylation. With the GPR161-S429A/S430A mutant, however, we detected no phosphorylation signal at all, underlining that S429/S430 is the target for PKA phosphotransferase activities (**Fig. 3b, Supplementary Fig. 7a**). Moreover, the L465P receptor mutant - which does not compartmentalize PKA complexes - showed a significant reduction of GPR161 phosphorylation following cAMP-elevation (**Fig. 3b**). The PKA mediated phosphorylation of GPCR-CT is regarded as one general principal of controlling GPCR desensitization[8, 9, 42, 43]. Therefore, these data underline that the GPR161 compartmentalized type I PKA activities directly sense and integrate cAMP-oscillations which affect receptor phosphorylation and localization. To underline that the CT is critical for cellular GPR161:PKA complexes we used the Venus-YFP tagged receptor constructs for co-precipitation studies. In immunoprecipitations of GPR161-wt we co-purified cAMP-dependent PKA complexes. The GPR161-ΔCT variant showed no PPI with PKA subunits

(**Supplementary Fig. 7b**). The same constructs were tested in localization studies. The wild type receptor and the S429A/S430A mutant were mainly localized to cytoplasmic compartments. In agreement with previous studies [33] the GPCR161 variant which lacks the CT (GPR161-ΔCT) was primarily localized to the plasma membrane (**Supplementary Fig. 7c**). To ease co-localization studies with RIα-GFP we tagged full length receptors at the carboxy terminus with mCherry. Following transient overexpression of the GPR161 variants in single transfection studies we confirmed cytoplasmic accumulations of the receptor with all three used mutants. RIα-GFP was found throughout the cytoplasma with highly specific speckled/punctuate localizations (**Fig. 3c**). Interestingly, upon co-expression of the wt and SS429AA receptor the a proportion of the GPR161:RIα complex was recruited to the plasma membrane. Strikingly, with the GPR161-L465P mutant we detected no co-localization nor membrane recruitment (**Fig. 3d**). These data underline an involvement of RI subunit binding in membrane targeting of GPR161.

The involvement of GPR161 in cilium signaling has been shown previously. Therefore we determined the localization of GPR161:RIα directly in Zebrafish embryos. We observed that overexpression of the mCherry tagged wild type GPR161initiated receptor mediated PKA recruitment into the primary cilium of zebra fish embryos. In the experiments with the L465P mutant we observed significantly less cilium staining of GFP tagged RIα (**Fig. 3e Pia your turn**).

Next we applied a *Renilla* luciferase (*R*luc) based protein-fragment complementation assay (PCA) to confirm that binary GPR161:RI interactions are formed directly in the living cell (**Fig. 4a**). Besides quantification of RIα homodimer formation we illustrate specific binding of RIα to GPR161 in HEK293 cells. With the GPR161-L465P mutant the PPI signal decreased significantly (**Fig. 4b**). To our surprise we also detected GPR161 dimerization using this cellular PPI reporter. Application of L465P mutants rather showed an increase of GPR161 dimers. However, the functional consequence of this observation needs to be evaluated. As predicted we observed that elevation of cAMP-levels triggered PKA complex dissociation of RIα:PKAc. We could not detect a major impact of cAMP elevation on the GPR161:RIα complex (**Supplementary Fig. 8**). We also wanted to test how far disease mutations of RIα and RIβ affect the complex formation with the AKAP GPR161.

Through the N terminal dimer and docking domain, R subunit dimerizes and interacts with amphipathic helices of AKAPs[14, 44]. Therefore a perturbation of the integrity of the dimer and docking region would specifically affect AKAP interaction. Recently the patient mutation L50R in the D/D region of RIβ has been associated with a neurodegenerative disorder causing accumulations of RIβ in neuronal inclusions[27]. Using the *R*luc PCA reporter we showed that RIβ specifically binds to GPR161. Application of the RIβ[L50R] mutant significantly decreased RIβ homo-dimerization (**Fig. 4c**). It is the amino acid substitution directly in the antiparallel four helix bundle in the dimer/docking of RIβ dimers which is responsible for complex disruption. Dimer formation of R subunits is also a precondition for AKAP binding. In the *R*luc PCA measurements we observed a substantial reduction of RIβ[L50R]:GPR161 complexes (**Fig. 4c**). This experiment further underlines that GPR161 acts as type I AKAP. Next, we also wanted to test a link to better characterized patient mutations in the *PRKAR1A* gene. A collection of RIα mutations have been linked to distinct disease phenotypes[17, 20, 24-26, 45-50]. In the recent years a growing number of RIα–disease mutations from Acrodysostosis and Carney complex patients have been made public. In contrast to perturbations of R dimerization, the tested RIα mutations either affect cAMP binding or - in the case of the Carney complex mutant R74C - the mode of action is still controversial. We quantitatively evaluated the impact of all three RIα mutations by analyzing complex formation with GPR161. We showed that neither the Carney complex mutation (R74C) nor the Acrodysostosis mutations (R335P, R368X) significantly changed the complex formation with GPR161 (**Fig. 4d**). This underlines that the GPR161:RIα complexes are formed despite the mutations. However, what is the functional consequence of mutational perturbation of cAMP nucleotide binding domain B (CNBB)? Using the *R*luc PCA as read out we showed that the RIα[R335P] mutated PKA type I complex (which actually still interacts with GPR161) is less responsive to beta-adrenergic receptor initiated cAMP-elevations (**Fig. 4d**). The R335P mutation is sufficient to impair the cAMP-dependent dissociation of PKAc from RIα. These data underline that GPR161 binds mutated RI holoenzyme complexes which are less reactive to cAMP controlled PKA activation. We assume that in a pathological cell setting such GPR161-anchored PKA complexes would be insensitive to transient cAMP-elevations thereby reducing or preventing PKA substrate phosphorylation.

Conclusion.

The idea that scaffolding proteins act as organizing centers to converge and redirect the information flow has evolved during the last two decades[4, 7]. Diverse scaffolds assemble flexible signaling nodes consisting of GTPases, kinases and phosphatases spatially and temporally. In the classical view scaffolds like the AKAP family, beta-arrestin, Ksr1 or PSD-proteins act as flexible connecting pieces between receptors and downstream effectors [1, 2, 4, 51]. Here we illustrate that one orphan GPCR by itself contains all the structural features that allow to be a high affinity anchoring protein (AKAP) for type I PKA. Several examples how selective AKAPs recruit type II PKA to distinct membrane receptors have been illustrated[14, 52, 53 54]. Here we present the discovery of a binary receptor-kinase interaction which opens new possibilities for anchoring and receptor-mediated compartmentalization of PKA contribute to physiological but also pathological receptor and kinase functions. This demonstrates that PKA type I compartmentalization is essential for efficient receptor phosphorylation which is a general principle for controlling receptor desensitization[8, 9, 42, 43]. An additional function of the binary GPR161-PKA interaction is the targeting of receptor-kinase complexes to the plasma membrane. The mode of action is still elusive. Interestingly, in a recent study GPR161 expression levels have been correlated with aberrant proliferation in triple negative breast cancer cells[37]. This observation and our findings that exclusively type I PKA regulatory subunits (RIα/β) bind to the membrane receptor motivated us to test GPR161 interactions with mutated and disease relevant RI subunits. Several genetic defects in distinct PKA subunits have been revealed. Both kinase inactivating and activating mutations have been described. Besides dysfunctions of phosphotransferase activities of PKAc which are linked to Cushing's syndrome and hepatocellular carcinoma [18, 19, 21, 23, 24] mutations of both RI subunits (RIα or RIβ) have been linked to distinct phenotypes: Inactivating *PRKAR1A* gene (RIα) mutations cause deregulated PKAc activities. Distinct mutations in RIα account for the generation of endocrine tumors and cortisol-producing adenomas as observed in a disorder called Carney Complex[45-47, 49, 50]. Specific *PRKAR1A* gene (RIα) mutations impair cAMP-dependent PKA activation and cause hormone resistance as observed in the rare disease Acrodysostosis (a form of skeletal dysplasia) [25, 26]. We showed that mutated RIα subunits as found in Carney Complex patients (RIα[R74C])[50]

and Acrodysostosis patients (RIα[R335P], RIα[R368X])[26, 48] still interact with GPR161 (Figure 4). Such an interaction would desensitize compartmentalized GPR161-PKA complexes for cAMP-activation in case of Acrodysostosis. In addition we showed that a point mutation in the *PRKAR1B* gene (RIβ[L50R]), which is associated with neurodegenerative diseases[27], diminished PPI with GPR161. We speculate that such a dominant negative function of RI subunits would dramatically decrease the complex formation of wild type RI subunits involved in dimer formation with the AKAP-receptor. Therefore we recommend that this new and high affinity RI scaffolding function of GPR161 needs to be considered in analyses of spatiotemporal cAMP-dynamics in diseases with PKA dysfunction.

Recent evidence illustrated that localized GPR161 functions are associated with hedgehog signaling in the primary cilium[34]. Indeed, we showed in a model organism that GPR161 targets RIα to the cilium. Primary cilia are platforms for seven-transmembrane spanning receptor cascades including the hedgehog-linked smoothened pathway (Smo), which antagonizes cAMP-signaling. GPR161 activities seem to be the long-sought factors for creating spatiotemporal controlled cAMP-gradients in the ciliary hedgehog signaling pathway[55, 56]. In the primary cilium compartment cAMP-elevating GPR161 activities negatively regulate hedgehog signaling. Interestingly, activation of the counteracting hedgehog pathway triggers the removal of GPR161 from the cilium[34]. Our discovery has considerable consequences for the cilium signaling: First, the AKAP motif embedded within the GPR161 tail recruits and compartmentalizes cAMP-sensing type I holoenzymes into the plasma membrane of the cilium. Second, hedgehog ligands antagonize ciliary pools of GPR161 and most probably also receptor-interacting PKA activities. Overall we believe that the ciliary signaling complex consisting of cAMP-sensing GPR161-PKA is the missing link to integrate cAMP levels, compartmentalized PKA activities, and counteracting Smo signaling. A variety of ciliary dysfunctions, termed ciliopathies have been described[55, 57]. Both, the involvement of spatiotemporal cAMP-dynamics and the integrity of GPR161-PKA complexes need to be considered in molecular analyses of selected ciliopathies. In this context the smoothened receptor, a key component of seven-transmembrane receptors signaling in the primary cilium, is already a central target for cancer drug discovery efforts[58]. We assume that pharmacological targeting of the AKAP

and/or the receptor function of the G-alpha-s coupled GPR161 receptor is one strategy to redirect decontrolled cAMP signaling. We hypothesize that besides direct pharmacological perturbation of receptor or kinase activities the ubiquitination of receptor interacting RI subunits is a feasible and alternative approach for controlling GPR161-PKA localization and signaling. Praja2 has been recently identified to be the major E3 ligase for PKA RI subunit ubiquitination[59]. It has been shown that PKA activities enhance praja2 mediated degradation of phosphotransferase inhibitory PKA RI subunits leading to enhanced PKAc activities[59]. We speculate that degradation of R subunits is an alternative direction to impact GPR161 signaling. Taken together, we propose that the binary GPR161-PKA complex is a compartmentalized signaling hub that directly integrates receptor-sensed input signals with spatiotemporal cAMP dynamics. So far GPR161 is the first GPCR shown to have an AKAP function. Given that GPCRs are the largest family of cell surface molecules involved in signal transmission, it would be surprising if GPR161 is the 'lone wolf' with AKAP function amongst more than 800 GPCRs in the human genome [60]. However, if this is the case then it would further emphasize its critical and kinase-compartmentalizing receptor function.

Figure legends:

Figure 1: PKA phospho-protein interactome and GPR161:RI interaction. a, Phospho-proteins of affinity-purified PKA complexes are listed. A total of 127 phosphorylated amino acid residues isolated using PKA selective cAMP-resin are indicated; underlining marks previously described p-sites; red labeling highlights PKA group sites with a phosphorylated RxxS/T sequence motif. Potential cAMP binding proteins are indicated (*). **b,** Schematic illustration of GPR161 trafficking and signaling. **c,** GST pulldown analyzes of endogenous PKA subunits from HEK293 cell lysates in the presence or absence of 5 mM cAMP using GST and GST-CT (GPR161-*Carboxy-Terminus*$^{342-529}$) fusions. **d,** Spotted peptides (25 mers, 20 aa [amino acid] overlap) of GPR161-*CT*$^{342-529}$ were overlaid with recombinant RIα (Coomassie Brilliant Blue staining is shown). Immunoblotting (IB) has been performed with a monoclonal anti-RI antibody. **e,** Helical wheel projection of the identified amphipathic helix (aa 452…469) and indication of the centered L465 aa.

Figure 2: Interactions of GPR161:RIα *in vitro* and *in silico*. a, GST pulldown analyzes of recombinant RIα in the presence or absence of 5 mM cAMP using indicated GST-CT fusions of GPR161 including the *CT*$^{342-529}$-L465P mutant. **b,** Following bacterial co-expression of hexa-histidin (*his*^{6}) and s-tag tagged *CT*$^{378-529}$ (wt and L465P) and untagged RIα (schematics are shown) we purified complexes using Ni-NTA resin. A representative CBB stained gel from n=3 independent experiments is shown. **c.** Structure-based alignment of GPR161 with RI specific and dual specific AKAPs. Residues that are similar and bind the D/D domain hydrophobic groove are shown in red. Identity (*) and similarities (: .) are indicated. Leucins highlighted with a red box are shown in the structure model in f. **d.** Structural model of RIα D/D domain in complex with GPR161-*CT*$^{457-479}$ peptide. Crystal structure of RIα D/D domain in complex with DAKAP-2 peptide (PDB accession number 3IM4) was used to build the model in PyMol. The DAKAP-2 sequence was substitute with predicted amphipathic helix sequence of GPR161-*CT*$^{457-479}$. Side and top view of the model are shown. The monomers of the RIα D/D domain are depicted in gold and yellow and the GPR161 helix is shown in red. The GPR161 residues that dock onto the hydrophobic groove formed by the two RIα monomers are represented as surfaces. **e.** Direct binding of full-length RIα (●) or full length RIIβ (■) to FAM-labeled amphipathic helix of GPR161 (excitation at 535mm and emission at 580nm) by steady-state fluorescence anisotropy measurements. Shown is the amalgamated data from n=3 independent experiments. K_D value: 6.039 nM (±0.105). **d.** Model of RIa D/D domain in complex with GPR161 (457-479): Enlarged elements of GPR161 (L459 [part of the N-cap] and L477 [part of the C-cap]) interact with disulfide bridges from D/D RIα subunits.

Figure 3: Compartmentalization and phosphorylation of GPR161:RIα complexes. a. Schematic illustration of GPR161 with the phosphorylation site and the core AKAP motif (with the centered LAKAI sequence) located in the CT. **b.** Immunoprecipitation of Venus-YFP tagged GPR161 variants expressed in HEK293 cells following treatments with Forskolin (20 µM, 10 min) and Isoproterenol (1 µM, 10 min). Densitometry was used to quantification average changes of GPR161 phosphorylation (n=4 independent experiments, ±SEM). We used a phospho-(K/R)(K/R)X(S*/T*) specific antibody to analyze PKA phosphorylation [*] (Cell Signaling; #9621). IB from RI is from a different experiment

(it shows a better separation of antibody and RI). **c.** Subcellular localization of Venus-YFP tagged GPR161 fusion proteins in HEK293 cells. **d.** Subcellular localization of coexpressed mCherry-tagged GPR161 variants (wild type, L465P, SS429/430AA) and GFP-tagged RIα in HEK293 cells. **e.** Sequence alignment of the GPR161 CT and localization of GFP-tagged RIα and mCherry-tagged GPR161 in sections from zebra fish embryos. **f.** Quantification of cilia showing co-localizations of GPR161 variants and RIα.

Figure 4: Altered PPI of GPR161 variants with wild type and mutated RI. a. Schematic illustration of the *R*luc-PCA biosensor strategy to quantify PPI of wild type and mutated GPR161 and RI *in vivo*. **b.** Impact of L465P mutation of GPR161-F[1]/[2] on complex formation with RIα-F[1]/[2] (±SEM; representative of n=3). **c.** Impact of the L50R disease mutation found in neurodegenerative diseases on RIβ:GPR161 interaction measured using the *R*luc PCA (±SEM; representative of n=3). **d.** Impact of patient mutations from Acrodysostosis (R335P, R368X) and Carney complex (R74C) patients on binary interaction with GPR161-F[2] (±SD; average of n=3 independent experiments). **e.** The effect of increasing isoproterenol (15 min) concentrations on PKA complex formation using indicated *R*luc PCA expression vectors has been determined using transiently transfected HEK293 cells stably expressing the β_2AR (average of n=4 independent experiments, ±SEM).

Supplementary information.

Supplementary Figure 1: Strategy to isolate endogenous PKA complexes using a PKA specific cAMP-agarose resin. a. Structure of Rp-8AHA-cAMP agarose. **b.** Flow chart of the proteomics and phospho-proteomics approach. Affinity-isolated PKA complexes from U2OS cells were analyzed using LC-MS/MS followed by semi-quantitatively interrelationship analyses. **c.** Selective enrichment of endogenous PKA subunits from the osteosarcoma cell line U2OS. As negative control, we added excess of cAMP to mask cAMP-binding sites in R subunits for precipitation. Potential AMP binders are indicated (*).

Supplementary Figure 2: PPI network emanating from PKA. Following phospho-proteomic analyses using LC-MS/MS, we generated a static PPI network of the confident set of PKA interacting proteins. We neglected applied pharmacological applications for the construction of the macromolecular PKA PPI network. Dark lines indicate known interactions. Triangles indicate identified phosphopeptides; circles indicate identified peptides; squares indicate identified peptides and phosphopeptides from the same protein or protein isoform.

Supplementary Figure 3: Biochemical interaction studies of GPR161 and PKA. a. GST pulldown analyzes of endogenous PKA subunits from HEK293 cell lysates in the presence or absence of 5 mM cAMP using GST and GST-CT variants. **b.** cAMP-precipitation of endogenous PKA complexes and overexpressed GPR161 variants tagged with Venus-YFP using two types of cAMP agarose. We have enriched PKA holoenzyme complexes using Rp-8-AHA-cAMP and activated PKA regulatory complexes using 8-AHA-cAMP. In the negative control experiment we added excess of cAMP (5 mM) to the lysates to mask the cAMP binding sites in the R subunits for precipitation.

Supplementary Figure 4: Bacterial expression and interaction analyzes of GPR161-CT and RIα. Following bacterial co-expression of hexa-histidin (*his*^{6}) and s-tag tagged *CT*$^{378\text{-}529}$ (wt and L465P) and untagged RIα (schematics are shown) we purified complexes using Ni-NTA resin. Subsequently to imidazol elutions *CT*$^{378\text{-}529}$ bound complexes have been subjected to cAMP precipitations (± excess of cAMP; 5 mM).

Supplementary Figure 5: AKAP-peptide:RIα interactions. Spotted peptide sequences directly derived from amphipathic helices of indicated AKAPs or *in silico* designed peptides[39, 61] (25 mers, 20 aa [amino acid] overlap) were overlaid with recombinant RIα. We have integrated proline mutations to control RIα binding. Immunoblotting (IB) has been performed with a monoclonal anti-RI antibody.

Supplementary Figure 6: Amphipathic helix and RII specific AKAPs. a. Helix propensity prediction of GPR161 were measured with AGADIR - an algorithm to predict the helical content of peptides. **b.** Structure-based alignment of RII specific AKAPs. Residues that are similar and bind the D/D domain hydrophobic groove are indicated (:).

Supplementary Figure 7: Immunoprecipitation, phosphorylation and localization of of GPR161. a. Immunoprecipitation of Venus-YFP tagged GPR161 variants expressed in HEK293 cells (representative of n=3). **b.** Immunoprecipitation of Venus YFP tagged GPR161 variants expressed in HEK293 cells following treatments with Forskolin (20 µM, 10 min; representative of n=3). We used a phospho-(K/R)(K/R)X(S*/T*) specific antibody to analyze PKA phosphorylation [*] (Cell Signaling; #9621). **c.** Subcellular localization of Venus-YFP tagged GPR161 fusion proteins in HEK293 cells.

Supplementary Figure 8: Impact of Forskolin on PPI of GPR161 dimers and GPR161:RIα. Following coexpression of indicated *R*luc PCA tagged constructs in HEK293 cells and subsequent Forskolin exposure (15 min, 20µM) bioluminescence signals have been quantified using the *R*luc PCA as read out.

Supplementary table 1. Summary of peptides and phosphopeptides from the phospho-proteomics analyses (on the following 7 pages).

Methods.

Cell culture and antibodies. HEK293 and U2OS cells were grown in DMEM supplemented with 10% FBS. Transient transfections were performed with Transfectin reagent (Biorad). Cells were treated with Forskolin (Biaffin) or Isoproterenol (Sigma) with indicated concentrations and for the indicated time frames. Primary antibodies used were mouse anti-PKAc (BD Bioscience, #610981), anti-RIIβ (BD Bioscience, # 610626), anti-RI (BD Bioscience, #610166), anti-Rluc antibodies (MAB4400 versus Rluc-F(2), MAB4410 versus Rluc-F(1); Chemicon), anti-GST (Sigma, # G1160), anti-GFP (Roche, #11814460001) anti-GPR161 (Abcam, #83007; worked just with recombinant proteins), and a phosphospecific antibody to analyze PKA phosphorylation [*; (K/R)(K/R)X(S*/T*)] (Cell Signaling; # 9621).

cAMP-agarose protein precipitation assay. We isolated endogenous protein complexes from U2OS cells under five conditions: for baseline binding and control of

binding specificity, without stimulation (i) and in the presence of excess of cAMP (ii), respectively. In parallel we performed PKA isolations following Forskolin stimulation for ten minutes (iii) and Isoproterenol for ten minutes (iv) and 24 hours (v). Following treatment with Forskolin (50 µM; 10 min) or Isoproterenol (10 µM; 10 min, 24 h [twice: at the time points 0 and 12 hour]) U2OS cells were homogenized using a Potter S (B. Braun Biotech International) with 15 strikes (standard lysis buffer: 10 mM sodium phosphate pH 7.2, 150 mM NaCl, 0.5% Triton-X100 supplemented with standard protease inhibitors and phosphatase inhibitors). We clarified the lysate (13 000 rpm, 15 min) and precipitated endogenous PKA regulatory subunit associated protein complexes with PKA selective Rp-8-AHA-cAMP agarose resin (Biolog, #A012) for two hours at 4°C. As negative control experiment we added excess of cAMP (1 mM) to the lysates to mask the cAMP binding sites in the R subunits for precipitation. Resin associated proteins were washed four times with standard lysis buffer and eluted with 1% SDS. Following SDS removal (using SDS removal columns; Calbiochem, # 263454) we analyzed the proteomic and phospho-proteomic composition of bead associated complexes as previously described [62]. We followed the same cAMP-precipitation protocol following transient overexpression of GPR161 variants in HEK293 cells. This time resin associated proteins were subjected to SDS-polyarylamid gel electrophoresis followed by immunoblotting.

LC-MS/MS analyses. We were interested in both protein identity and protein phosphorylation: therefore we split the samples (83-250 µg each) and enriched 80% of the trypsin-digested material with titanium dioxide for phospho-peptide identification. The remaining 20% of the isolated material was used for the identification of bound proteins using LC-MS/MS. All experiments were performed as independent experiments and/or as independent triplicates. Tryptic digests and enriched phosphopeptides were analyzed on the LTQ-Orbitrap XL mass spectrometer (Thermo Fischer Scientific) coupled to a nano-flow LC system (Eksigent). Peptides were first trapped on a reverse-phase pre-column (4mm length, 360 mm i.d.) and then separated on the analytical column (10 cm length, 150 mm i.d.) (Jupiter C18, 3mm, 300 Angstrom (A°), Phenomenex) using an acetonitrile gradient ranging from 2 to 33% over 53 min at 600 nL/min. MS instrument was operated with the nano-electrospray source voltage set to 1.7 kV, MS scan resolution to 60 000 (lock mass activated) and CID MS/MS spectra were acquired on data-dependent

acquisition mode for the three most abundant precursor ions (5 000 counts intensity threshold) [62].

MS data processing. Acquired MS/MS spectra were pre-processed with Mascot Distiller v2.1.1 (Matrix Science) and the generated MGF files were searched with Mascot 2.1 on a concatenated target/decoy IPI human database v3.37 (34 584 protein sequences). Search parameters were as follow: precursor mass tolerance ±10 p.p.m., peptide fragment mass tolerance ±0.5Da, trypsin (two missed cleavages), and these variable modifications: carbamidomethyl (C), deamidation (NQ), oxidation (M), phosphorylation (STY). ProteoConnections, our in house bioinformatics software for phosphoproteomics analysis, was used to limit peptide FDR to 1%, to assess phosphorylation site localization confidence and to annotate previously reported phosphorylation sites. High abundant proteins were removed from the data (*i.e.* > 400000 copies per cell) [63], then label-free quantification of peptides was performed [62, 64]. Programs were implemented in Python1, with some analyzes conducted with R2.

Motif detection. We searched motifs with motif-x and we pre-aligned our identified phosphosites with a width of 15 amino acids as input and the IPI human proteome as background data [65].

***In vitro* protein binding assays.** We cloned coding regions of indicated aa stretches of the GPR161-CT (murine, ABO93465.1) into the pGEX-5X1 vector using flanking EcoRI/XhoI restriction sites. All GST-hybrid proteins were expressed in Escherichia coli (strains: BL21-DE3-RIL, Rosetta pLysS). Induction, cell lysis and affinity purification of hybrid proteins were performed as recommended by the supplier of the pGEX vectors (GE Healthcare). GST hybrid proteins (GST, GST-CT variants) immobilized on glutathione beads were incubated with cell lysates from HEK293 cells (DMEM medium supplemented with 10% FBS) for three hours. Resin-associated complexes were washed at least four times with the standard lysis buffer (10 mM sodium phosphate pH 7.2, 150 mM NaCl, 0.5% Triton X100) and eluted with Laemmli sample buffer (2% SDS, 50 mM Tris HCl pH 6.8, 0.2 mg/ml bromphenol blue, 0.1 M DTT, 10% (v/v) glycerol).

Protein expression and purification. To obtain the prokaryotic expression vectors pET11d-RIα-his6 and pET11d-RIα the human coding region (PKA RIα, NP 002725.1) was PCR-amplified using oligonucleotides with or without the C-terminal *his*^{6}-tag followed by insertion into the multiple cloning site of the pET11d vector (Stratagene). Expression of recombinant proteins was performed in the *Escherichia coli* strain Rosetta pLysS (Novagen) at 30°C for 6 hours in LB medium. We purified PKA RIα-*his*^{6} protein by affinity chromatography according to supplier's instructions for the Ni-NTA spin kit (Qiagen) followed by a size exclusion chromatography using an ÄKTA Superdex-75 gel filtration column (GE Healthcare). To obtain the double-his6 tagged prokaryotic expression vector construct pET30a-GPR161-*CT*$^{378-528}$, the murine coding region (GPR161, ABO93465.1) was PCR-amplified followed by insertion into the multiple cloning site (BglII/XhoI) of the pET30a vector (Novagen). The L465P mutations was inserted via site directed mutagenesis. Co-expression of untagged RIα and *his*^{6}-*CT*$^{378-528}$-*his*^{6} proteins were performed in Escherichia coli strain BL21-DE3-RIL at 30°C for 3 hours (1 mM IPTG) in LB medium containing both ampicillin and kanamycin antibiotics. Subsequently, the co-expressed proteins (RIα and *his*^{6}-*CT*$^{378-528}$-*his*^{6}) were affinity purified according to supplier's instructions for the Ni-NTA agarose (Qiagen) and subjected to SDS-polyacrylamide gelelectrophoresis.

SPOT synthesis and overlay experiments. Overlapping peptides of GPR161-CT or i or indicated peptides containing substitutions of conserved amino acids in the different AKAP sequences were SPOT-synthesized (synthetic peptide arrays on membrane supports) on distinct coordinates of a cellulose membrane (starting from the N-terminus of the selected protein - C terminus of the GPCRs - with amino acid 1-25 [coordinate A1], amino acid 6-30 [coordinate A2], etc.) [38]. Membranes equilibrated in TBST buffer (10 mM Tris, 150 mM NaCl, 0,05% Tween 20, pH 7,4) were overlaid with recombinant RIα (TBST supplemented with 5% non-fat dry milk). Interactions were detected with mouse anti-RI and secondary horseradish peroxidase antibodies by a procedure identical to immunoblotting (IB).

Structural Docking. Crystal structure of RIα dimerization and docking D/D domain (residues 13-62) in complex with Dual specific AKAP 2 (D-AKAP2) (PDB accession number 3IM4)[41] was used to predict how the amphipathic helix sequence of GPR161-*CT*$^{457-479}$ will dock onto RIa D/D domain. DAKAP-2 sequence was substitute with

GPR161-*CT*$^{457-479}$ sequence (SLDSYAASLAKAIEAEAKINLFGEE) The model and the figures were generated in PyMol.

Fluorescence polarization. Full length PKA RIα and PKA RIIβ were purified as described previously[66, 67]. The 5- FAM N-terminal tagged GPR161 peptide (SLDSYAASLAKAIEAEAKINLFGEE), synthesized at NeoScientific (Cambridge, MA) and was dissolved in 100% DMSO. Serial dilutions of concentrated stocks of either RIa or RIIb purified proteins were prepared by diluting the proteins with the peptide in buffer A (10mM Hepes pH 7.4. 150mM NaCl, 3mM EDTA, 0.005% Surfactant P20). The final concentration of the peptide was 2nM. Samples were equilibrated for 10min or 1 hour at 25°C with no significant change in anisotropy signal observed for up to 1hour after sample preparation. Flat bottom black 96-well plates (Thermo) were used and the peptide was excited (535nm) and emission was monitored (580nm) by Tecan Genios Pro 96/384 Multifunction Microplate Reader (Tecan). Three separate binding experiments were averaged and fit to the non-linear regression model in GraphPad Prism version 6.0.

Zebra fish. Pia.

Immuno-precipitation. Following transient overexpression of indicated GPR161 variants tagged with Venus YFP we treated the cells either with Forskolin or Isoproterenol for indicated time frames. Subsequent to PBS washing steps we homogenized them using a Potter S (B. Braun Biotech International) with 15 strikes (standard lysis buffer: 10 mM sodium phosphate pH 7.2, 150 mM NaCl, 0.5% Triton-X100 supplemented with standard protease inhibitors and phosphatase inhibitors). We clarified the lysate (13 000 rpm, 15 min) and performed immunoprecipitations using ProteinA/G mixtures and 2 µg of control and anti-GFP antibodies for three hours at 4°C. Resin associated proteins were washed four times with standard lysis buffer and eluted with Laemmli sample buffer.

Imaging. Life cell imaging have been performed using a Leica TCS SP5 II inverse laser scanning microscope. The settings for co-localization experiments were as followed: Johanna Even following single transient transfections (24h, 48h) we examined both mCherry and GFP fluorescence to control specificity of excitation and emission.

***Renilla* luciferase PCA.** The *R*luc PCA based hybrid proteins RIIb-F[1] and PKAc-F[2] have been designed as previously described [68]. *R*luc PCA fusions GPR161 have been generated using an analogous cloning approach. Following PCR amplification of the of the GPR161 gene we fused them C-terminally with either -F[1] or -F[2] of the *R*luc PCA. PKA subunits and PKI were subcloned into the 5`end the 10aa linker $(GGGGS)_2$ and the *R*luc PCA fragments (pcDNA3.1 backbone vector). We generated the different mutants (RIα,β; GPR161) using site directed mutagenesis. HEK293 cells were grown in DMEM supplemented with 10% FBS. We transiently overexpressed indicated versions of the *R*luc-PCA based biosensor in 24 well plate format. 24 or 48 hours post-transfection we exchanged growth medium and resuspended cells in PBS. Cell suspensions were transferred to 96-well plates and subjected to bioluminescence analysis using the LMaxTM^{II}384 luminometer (Molecular Devices). Rluc bioluminescence signals were integrated for 10 seconds following addition of the Rluc substrate benzyl-coelenterazine (5 µM; Nanolight).

Acknowledgements: We thank Jim Millonig for providing the GPR161 cDNAs for cloning. We thank Adi Sandbichler for the help with the imaging platform and Karl Maly for the support with biacore measurements. We thank Sonja Geisler and Andrea Schraffl for technical and Gabi Reiter for management support. This work was supported by grants from the Austrian Science Fund (FWF; P22608, P27606 and SFB-F44).

Author contributions: VB, JEM, RI, RR, PR, MC, PMT, PA, US, ES performed the experiments. VB, JEM, RI, RR, PR, MC, PMT, PA, US, SST, ES analyzed the results. GSB contributed analytical tools. ES conceived the project and wrote the manuscript.

Competing financial interests

The authors declare no competing financial interests.

Supporting Information:

Supporting Table 1

Supporting Fig.1-8

References.

1. Langeberg, L.K. & Scott, J.D. Signalling scaffolds and local organization of cellular behaviour. *Nat Rev Mol Cell Biol* **16**, 232-244 (2015).
2. Shukla, A.K., Xiao, K. & Lefkowitz, R.J. Emerging paradigms of beta-arrestin-dependent seven transmembrane receptor signaling. *Trends in biochemical sciences* **36**, 457-469 (2011).
3. Rajagopal, S., Rajagopal, K. & Lefkowitz, R.J. Teaching old receptors new tricks: biasing seven-transmembrane receptors. *Nature reviews* **9**, 373-386 (2010).
4. Good, M.C., Zalatan, J.G. & Lim, W.A. Scaffold proteins: hubs for controlling the flow of cellular information. *Science (New York, N.Y* **332**, 680-686 (2011).
5. Ritter, S.L. & Hall, R.A. Fine-tuning of GPCR activity by receptor-interacting proteins. *Nat Rev Mol Cell Biol* **10**, 819-830 (2009).
6. Scott, J.D., Dessauer, C.W. & Tasken, K. Creating order from chaos: cellular regulation by kinase anchoring. *Annu Rev Pharmacol Toxicol* **53**, 187-210 (2013).
7. Scott, J.D. & Pawson, T. Cell signaling in space and time: where proteins come together and when they're apart. *Science (New York, N.Y* **326**, 1220-1224 (2009).
8. Daaka, Y., Luttrell, L.M. & Lefkowitz, R.J. Switching of the coupling of the beta2-adrenergic receptor to different G proteins by protein kinase A. *Nature* **390**, 88-91 (1997).
9. Tobin, A.B. G-protein-coupled receptor phosphorylation: where, when and by whom. *British journal of pharmacology* **153 Suppl 1**, S167-176 (2008).
10. Rockman, H.A., Koch, W.J. & Lefkowitz, R.J. Seven-transmembrane-spanning receptors and heart function. *Nature* **415**, 206-212 (2002).
11. Taylor, S.S., Ilouz, R., Zhang, P. & Kornev, A.P. Assembly of allosteric macromolecular switches: lessons from PKA. *Nat Rev Mol Cell Biol* **13**, 646-658 (2012).
12. Herberg, F.W., Maleszka, A., Eide, T., Vossebein, L. & Tasken, K. Analysis of A-kinase anchoring protein (AKAP) interaction with protein kinase A (PKA) regulatory subunits: PKA isoform specificity in AKAP binding. *Journal of molecular biology* **298**, 329-339 (2000).
13. Kinderman, F.S. *et al.* A dynamic mechanism for AKAP binding to RII isoforms of cAMP-dependent protein kinase. *Mol Cell* **24**, 397-408 (2006).
14. Wong, W. & Scott, J.D. AKAP signalling complexes: focal points in space and time. *Nat Rev Mol Cell Biol* **5**, 959-970 (2004).
15. Dessauer, C.W. Adenylyl cyclase--A-kinase anchoring protein complexes: the next dimension in cAMP signaling. *Molecular pharmacology* **76**, 935-941 (2009).
16. Houslay, M.D. Underpinning compartmentalised cAMP signalling through targeted cAMP breakdown. *Trends in biochemical sciences* (2009).
17. Stratakis, C.A. cAMP/PKA signaling defects in tumors: genetics and tissue-specific pluripotential cell-derived lesions in human and mouse. *Mol Cell Endocrinol* **371**, 208-220 (2013).
18. Beuschlein, F. *et al.* Constitutive activation of PKA catalytic subunit in adrenal Cushing's syndrome. *N Engl J Med* **370**, 1019-1028 (2014).
19. Sato, Y. *et al.* Recurrent somatic mutations underlie corticotropin-independent Cushing's syndrome. *Science (New York, N.Y* **344**, 917-920 (2014).
20. Espiard, S., Ragazzon, B. & Bertherat, J. Protein kinase a alterations in adrenocortical tumors. *Horm Metab Res* **46**, 869-875 (2014).
21. Cao, Y. *et al.* Activating hotspot L205R mutation in PRKACA and adrenal Cushing's syndrome. *Science (New York, N.Y* **344**, 913-917 (2014).
22. Cheung, J. *et al.* Structural insights into mis-regulation of protein kinase A in human tumors. *Proceedings of the National Academy of Sciences of the United States of America* **112**, 1374-1379 (2015).

23. Honeyman, J.N. *et al.* Detection of a recurrent DNAJB1-PRKACA chimeric transcript in fibrolamellar hepatocellular carcinoma. *Science (New York, N.Y* **343**, 1010-1014 (2014).
24. Zilbermint, M. & Stratakis, C.A. Protein kinase A defects and cortisol-producing adrenal tumors. *Current opinion in endocrinology, diabetes, and obesity* **22**, 157-162 (2015).
25. Silve, C., Clauser, E. & Linglart, A. Acrodysostosis. *Horm Metab Res* **44**, 749-758 (2012).
26. Linglart, A. *et al.* Recurrent PRKAR1A mutation in acrodysostosis with hormone resistance. *N Engl J Med* **364**, 2218-2226 (2011).
27. Wong, T.H. *et al.* PRKAR1B mutation associated with a new neurodegenerative disorder with unique pathology. *Brain* **137**, 1361-1373 (2014).
28. Stork, P.J. & Schmitt, J.M. Crosstalk between cAMP and MAP kinase signaling in the regulation of cell proliferation. *Trends Cell Biol* **12**, 258-266 (2002).
29. Dumaz, N. & Marais, R. Integrating signals between cAMP and the RAS/RAF/MEK/ERK signalling pathways. Based on the anniversary prize of the Gesellschaft fur Biochemie und Molekularbiologie Lecture delivered on 5 July 2003 at the Special FEBS Meeting in Brussels. *FEBS J* **272**, 3491-3504 (2005).
30. Gerits, N., Kostenko, S., Shiryaev, A., Johannessen, M. & Moens, U. Relations between the mitogen-activated protein kinase and the cAMP-dependent protein kinase pathways: comradeship and hostility. *Cellular signalling* **20**, 1592-1607 (2008).
31. Thaker, P.H. *et al.* Chronic stress promotes tumor growth and angiogenesis in a mouse model of ovarian carcinoma. *Nature medicine* **12**, 939-944 (2006).
32. Bensimon, A., Heck, A.J. & Aebersold, R. Mass spectrometry-based proteomics and network biology. *Annu Rev Biochem* **81**, 379-405 (2012).
33. Matteson, P.G. *et al.* The orphan G protein-coupled receptor, Gpr161, encodes the vacuolated lens locus and controls neurulation and lens development. *Proceedings of the National Academy of Sciences of the United States of America* **105**, 2088-2093 (2008).
34. Mukhopadhyay, S. *et al.* The ciliary G-protein-coupled receptor Gpr161 negatively regulates the Sonic hedgehog pathway via cAMP signaling. *Cell* **152**, 210-223 (2013).
35. Briscoe, J. & Therond, P.P. The mechanisms of Hedgehog signalling and its roles in development and disease. *Nat Rev Mol Cell Biol* **14**, 416-429 (2013).
36. Varjosalo, M. *et al.* Interlaboratory reproducibility of large-scale human protein-complex analysis by standardized AP-MS. *Nature methods* **10**, 307-314.
37. Feigin, M.E., Xue, B., Hammell, M.C. & Muthuswamy, S.K. G-protein-coupled receptor GPR161 is overexpressed in breast cancer and is a promoter of cell proliferation and invasion. *Proceedings of the National Academy of Sciences of the United States of America* (2014).
38. Bachmann, V.A. *et al.* Reciprocal regulation of PKA and Rac signaling. *Proceedings of the National Academy of Sciences of the United States of America* **110**, 8531-8536 (2013).
39. Burgers, P.P., van der Heyden, M.A., Kok, B., Heck, A.J. & Scholten, A. A systematic evaluation of protein kinase A-A-kinase anchoring protein interaction motifs. *Biochemistry* **54**, 11-21 (2015).
40. Lacroix, E., Viguera, A.R. & Serrano, L. Elucidating the folding problem of alpha-helices: local motifs, long-range electrostatics, ionic-strength dependence and prediction of NMR parameters. *Journal of molecular biology* **284**, 173-191 (1998).
41. Sarma, G.N. *et al.* Structure of D-AKAP2:PKA RI complex: insights into AKAP specificity and selectivity. *Structure* **18**, 155-166 (2010).
42. Gainetdinov, R.R., Premont, R.T., Bohn, L.M., Lefkowitz, R.J. & Caron, M.G. Desensitization of G protein-coupled receptors and neuronal functions. *Annual review of neuroscience* **27**, 107-144 (2004).
43. Nobles, K.N. *et al.* Distinct phosphorylation sites on the beta(2)-adrenergic receptor establish a barcode that encodes differential functions of beta-arrestin. *Sci Signal* **4**, ra51 (2011).

44. Carr, D.W. *et al.* Interaction of the regulatory subunit (RII) of cAMP-dependent protein kinase with RII-anchoring proteins occurs through an amphipathic helix binding motif. *The Journal of biological chemistry* **266**, 14188-14192 (1991).
45. Bertherat, J. *et al.* Mutations in regulatory subunit type 1A of cyclic adenosine 5'-monophosphate-dependent protein kinase (PRKAR1A): phenotype analysis in 353 patients and 80 different genotypes. *The Journal of clinical endocrinology and metabolism* **94**, 2085-2091 (2009).
46. Groussin, L. *et al.* Molecular analysis of the cyclic AMP-dependent protein kinase A (PKA) regulatory subunit 1A (PRKAR1A) gene in patients with Carney complex and primary pigmented nodular adrenocortical disease (PPNAD) reveals novel mutations and clues for pathophysiology: augmented PKA signaling is associated with adrenal tumorigenesis in PPNAD. *American journal of human genetics* **71**, 1433-1442 (2002).
47. Horvath, A. *et al.* Mutations and polymorphisms in the gene encoding regulatory subunit type 1-alpha of protein kinase A (PRKAR1A): an update. *Human mutation* **31**, 369-379 (2010).
48. Lee, H. *et al.* Exome sequencing identifies PDE4D mutations in acrodysostosis. *American journal of human genetics* **90**, 746-751 (2012).
49. Salpea, P. & Stratakis, C.A. Carney complex and McCune Albright syndrome: an overview of clinical manifestations and human molecular genetics. *Mol Cell Endocrinol* **386**, 85-91 (2014).
50. Veugelers, M. *et al.* Comparative PRKAR1A genotype-phenotype analyses in humans with Carney complex and prkar1a haploinsufficient mice. *Proceedings of the National Academy of Sciences of the United States of America* **101**, 14222-14227 (2004).
51. Magalhaes, A.C., Dunn, H. & Ferguson, S.S. Regulation of GPCR activity, trafficking and localization by GPCR-interacting proteins. *British journal of pharmacology* **165**, 1717-1736 (2012).
52. Malbon, C.C., Tao, J. & Wang, H.Y. AKAPs (A-kinase anchoring proteins) and molecules that compose their G-protein-coupled receptor signalling complexes. *The Biochemical journal* **379**, 1-9 (2004).
53. Esseltine, J.L. & Scott, J.D. AKAP signaling complexes: pointing towards the next generation of therapeutic targets? *Trends Pharmacol Sci* **34**, 648-655 (2013).
54. Fraser, I.D. *et al.* Assembly of an A kinase-anchoring protein-beta(2)-adrenergic receptor complex facilitates receptor phosphorylation and signaling. *Curr Biol* **10**, 409-412 (2000).
55. Schou, K.B., Pedersen, L.B. & Christensen, S.T. Ins and outs of GPCR signaling in primary cilia. *EMBO reports* **16**, 1099-1113 (2015).
56. Wong, S.Y. & Reiter, J.F. The primary cilium at the crossroads of mammalian hedgehog signaling. *Curr Top Dev Biol* **85**, 225-260 (2008).
57. Fliegauf, M., Benzing, T. & Omran, H. When cilia go bad: cilia defects and ciliopathies. *Nat Rev Mol Cell Biol* **8**, 880-893 (2007).
58. Lappano, R. & Maggiolini, M. G protein-coupled receptors: novel targets for drug discovery in cancer. *Nature reviews* **10**, 47-60 (2011).
59. Lignitto, L. *et al.* Control of PKA stability and signalling by the RING ligase praja2. *Nature cell biology* **13**, 412-422 (2011).
60. Lagerstrom, M.C. & Schioth, H.B. Structural diversity of G protein-coupled receptors and significance for drug discovery. *Nature reviews* **7**, 339-357 (2008).
61. Alto, N.M. *et al.* Bioinformatic design of A-kinase anchoring protein-in silico: a potent and selective peptide antagonist of type II protein kinase A anchoring. *Proceedings of the National Academy of Sciences of the United States of America* **100**, 4445-4450 (2003).
62. Courcelles, M. *et al.* Phosphoproteome dynamics reveal novel ERK1/2 MAP kinase substrates with broad spectrum of functions. *Mol Syst Biol* **9**, 669 (2013).
63. Beck, M. *et al.* The quantitative proteome of a human cell line. *Mol Syst Biol* **7**, 549 (2011).

64. Courcelles, M., Lemieux, S., Voisin, L., Meloche, S. & Thibault, P. ProteoConnections: a bioinformatics platform to facilitate proteome and phosphoproteome analyses. *Proteomics* **11**, 2654-2671 (2011).
65. Schwartz, D. & Gygi, S.P. An iterative statistical approach to the identification of protein phosphorylation motifs from large-scale data sets. *Nat Biotechnol* **23**, 1391-1398 (2005).
66. Kim, C., Cheng, C.Y., Saldanha, S.A. & Taylor, S.S. PKA-I holoenzyme structure reveals a mechanism for cAMP-dependent activation. *Cell* **130**, 1032-1043 (2007).
67. Brown, S.H., Wu, J., Kim, C., Alberto, K. & Taylor, S.S. Novel isoform-specific interfaces revealed by PKA RIIbeta holoenzyme structures. *J Mol Biol* **393**, 1070-1082 (2009).
68. Stefan, E. *et al.* Quantification of dynamic protein complexes using Renilla luciferase fragment complementation applied to protein kinase A activities in vivo. *Proceedings of the National Academy of Sciences of the United States of America* **104**, 16916-16921 (2007).

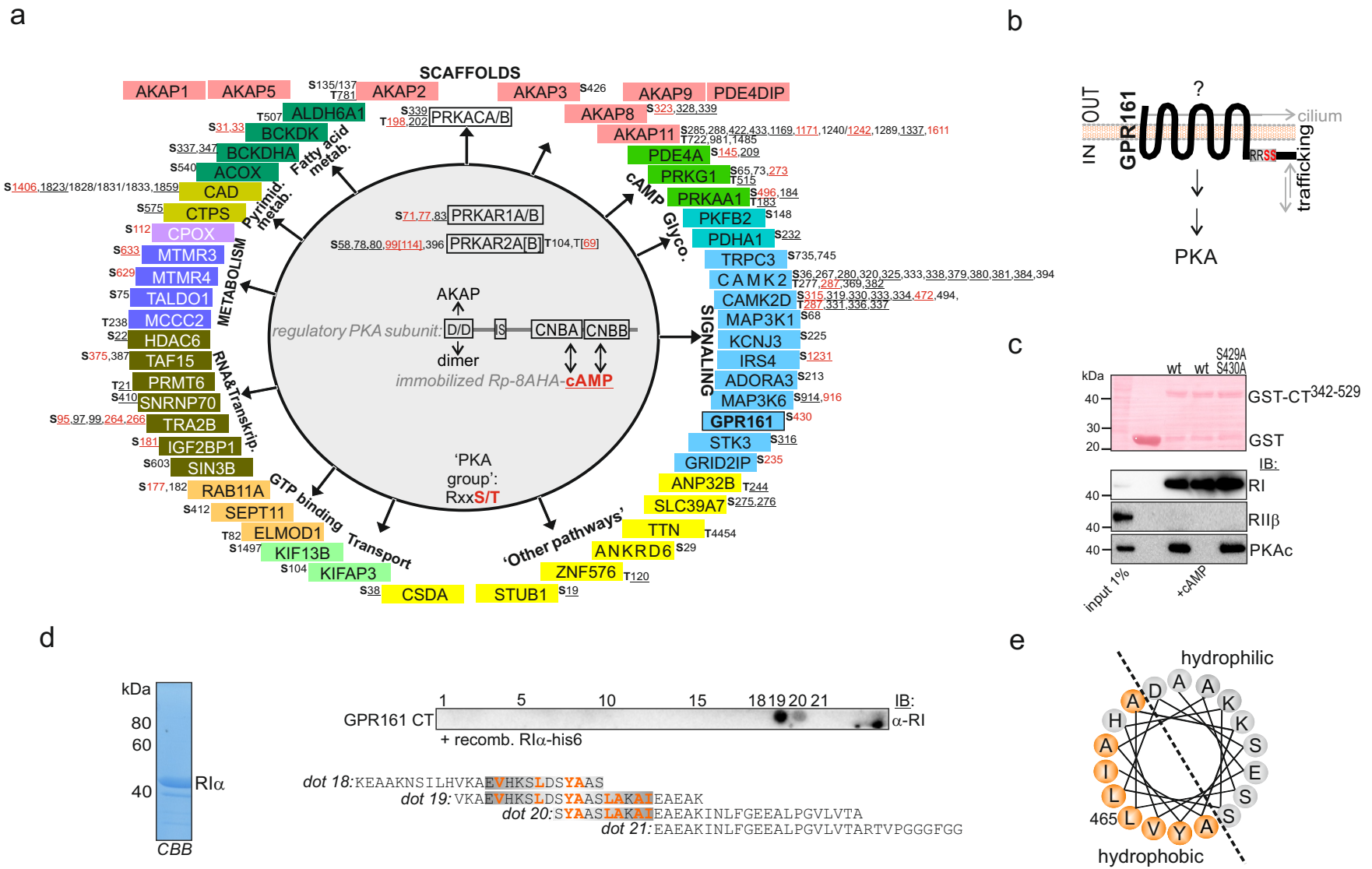
a
SCAFFOLDS
AKAP1
AKAP5
AKAP2
AKAP3
AKAP9
PDE4DIP
AKAP8
AKAP11
PRKACA/B
PRKAR1A/B
PRKAR2A[B]
AKAP
regulatory PKA subunit:
D/D
S
CNBA
CNBB
dimer
immobilized Rp-8AHA-cAMP
'PKA group': RxxS/T
METABOLISM
Fatty acid metab.
Pyrimid. metab.
Glyco.
cAMP
SIGNALING
RNA&Transkrip.
GTP binding
Transport
'Other pathways'
ALDH6A1
BCKDK
BCKDHA
ACOX
CAD
CTPS
CPOX
MTMR3
MTMR4
TALDO1
MCCC2
HDAC6
TAF15
PRMT6
SNRNP70
TRA2B
IGF2BP1
SIN3B
RAB11A
SEPT11
ELMOD1
KIF13B
KIFAP3
CSDA
PDE4A
PRKG1
PRKAA1
PKFB2
PDHA1
TRPC3
CAMK2
CAMK2D
MAP3K1
KCNJ3
IRS4
ADORA3
MAP3K6
GPR161
STK3
GRID2IP
ANP32B
SLC39A7
TTN
ANKRD6
ZNF576
STUB1
b
IN
OUT
GPR161
?
cilium
RRSS
trafficking
PKA
c
kDa
wt
wt
S429A S430A
40
30
20
GST-CT342-529
GST
IB:
RI
RIIβ
PKAc
input 1%
+cAMP
d
kDa
80
60
40
RIα
CBB
GPR161 CT
1
5
10
15
18 19 20 21
IB:
α-RI
+ recomb. RIα-his6
dot 18: KEAAKNSILHVKAEVHKSLDSYAAS
dot 19: VKAEVHKSLDSYASLAKAIEAEAK
dot 20: SYASLAKAIEAEAKINLFGEEALPGVLVTA
dot 21: EAEAKINLFGEEALPGVLVTARTVPGGGFGG
e
hydrophilic
hydrophobic
465

Figure 1

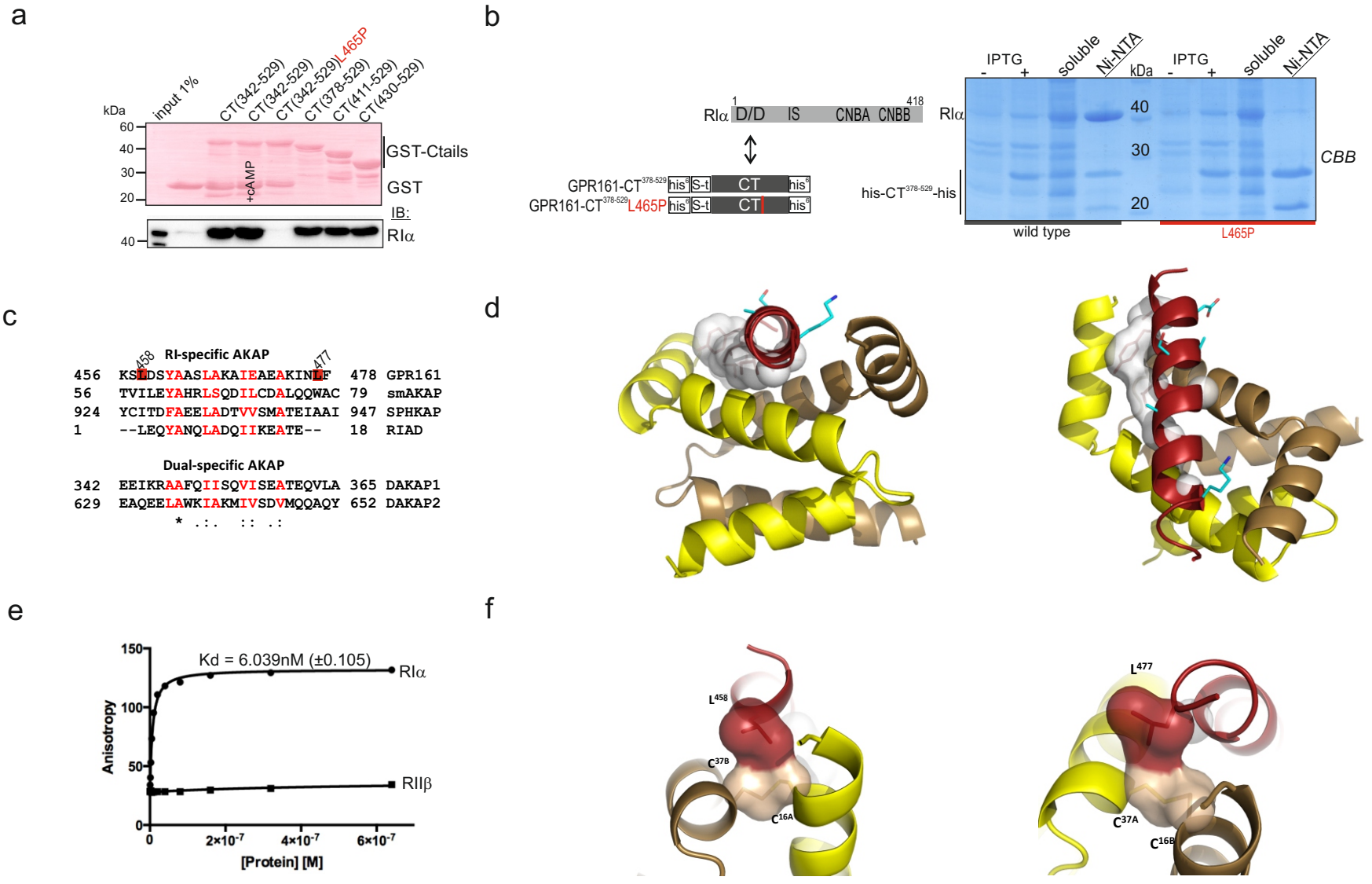
a
kDa
input 1%
CT(342-529)
CT(342-529)
CT(342-529)L465P
CT(378-529)
CT(411-529)
CT(430-529)
60
40
30
20
+cAMP
GST-Ctails
GST
IB:
RIα
40
b
RIα D/D IS CNBA CNBB
1
418
GPR161-CT378-529 his6 S-t CT his6
GPR161-CT378-529L465P his6 S-t CT his6
IPTG
soluble
Ni-NTA
kDa
RIα
40
30
20
CBB
his-CT378-529-his
wild type
L465P
c
RI-specific AKAP
458
477
456 KSLDSYAASLAKAIEAEAKINLF 478 GPR161
56 TVILEYAHRLSQDILCDALQQWAC 79 smAKAP
924 YCITDFAEELADTVVSMATEIAAI 947 SPHKAP
1 --LEQYANQLADQIIKEATE-- 18 RIAD
Dual-specific AKAP
342 EEIKRAAFQIISQVISEATEQVLA 365 DAKAP1
629 EAQEELAWKIAKMIVSDVMQQAQY 652 DAKAP2
* .:. :: .:
d
e
Kd = 6.039nM (±0.105)
RIα
RIIβ
Anisotropy
150
100
50
0
0
2×10-7
4×10-7
6×10-7
[Protein] [M]
f
L458
C37B
C16A
L477
C37A
C16B

Figure 2

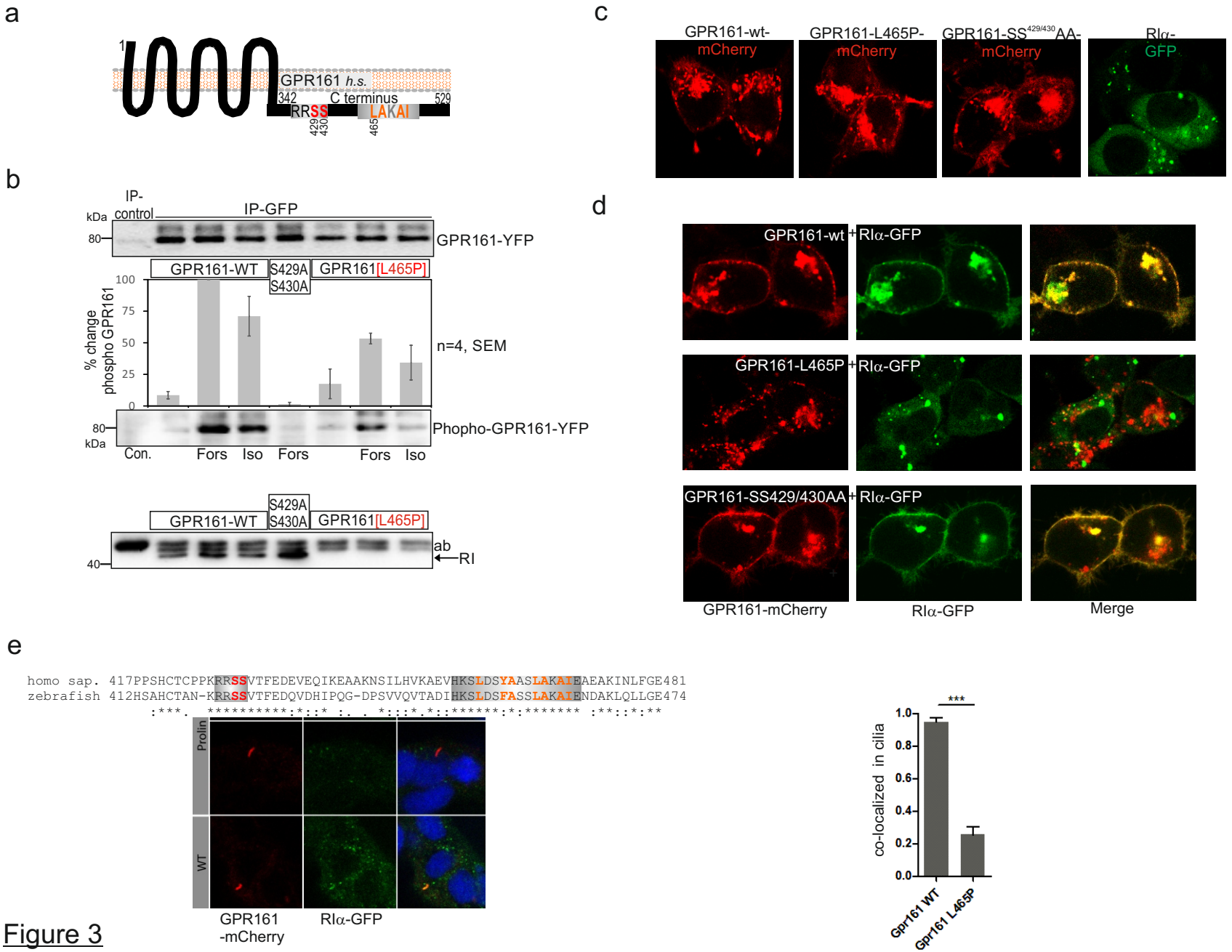
a
1
GPR161 h.s.
342
C terminus
529
RRSS
LAKAI
429
430
465
b
IP-
control
IP-GFP
kDa
80
GPR161-YFP
GPR161-WT
S429A
S430A
GPR161[L465P]
100
75
50
25
0
% change
phospho GPR161
n=4, SEM
80
kDa
Phopho-GPR161-YFP
Con.
Fors
Iso
Fors
Fors
Iso
S429A
S430A
GPR161-WT
GPR161[L465P]
40
ab
RI
c
GPR161-wt-
mCherry
GPR161-L465P-
mCherry
GPR161-SS429/430AA-
mCherry
RIα-
GFP
d
GPR161-wt +
RIα-GFP
GPR161-L465P +
RIα-GFP
GPR161-SS429/430AA +
RIα-GFP
GPR161-mCherry
RIα-GFP
Merge
e
homo sap. 417PPSHCTCPPKRRSSVTFEDEVEQIKEAAKNSILHVKAEVHKSLDSYAASLAKAIEAEAKINLFGE481
zebrafish 412HSAHCTAN-KRRSSVTFEDQVDHIPQG-DPSVVQVTADIHKSLDSFASSLAKAIENDAKLQLLGE474
Prolin
WT
GPR161
-mCherry
RIα-GFP
***
co-localized in cilia
1.0
0.8
0.6
0.4
0.2
0.0
Gpr161 WT
Gpr161 L465P

Figure 3

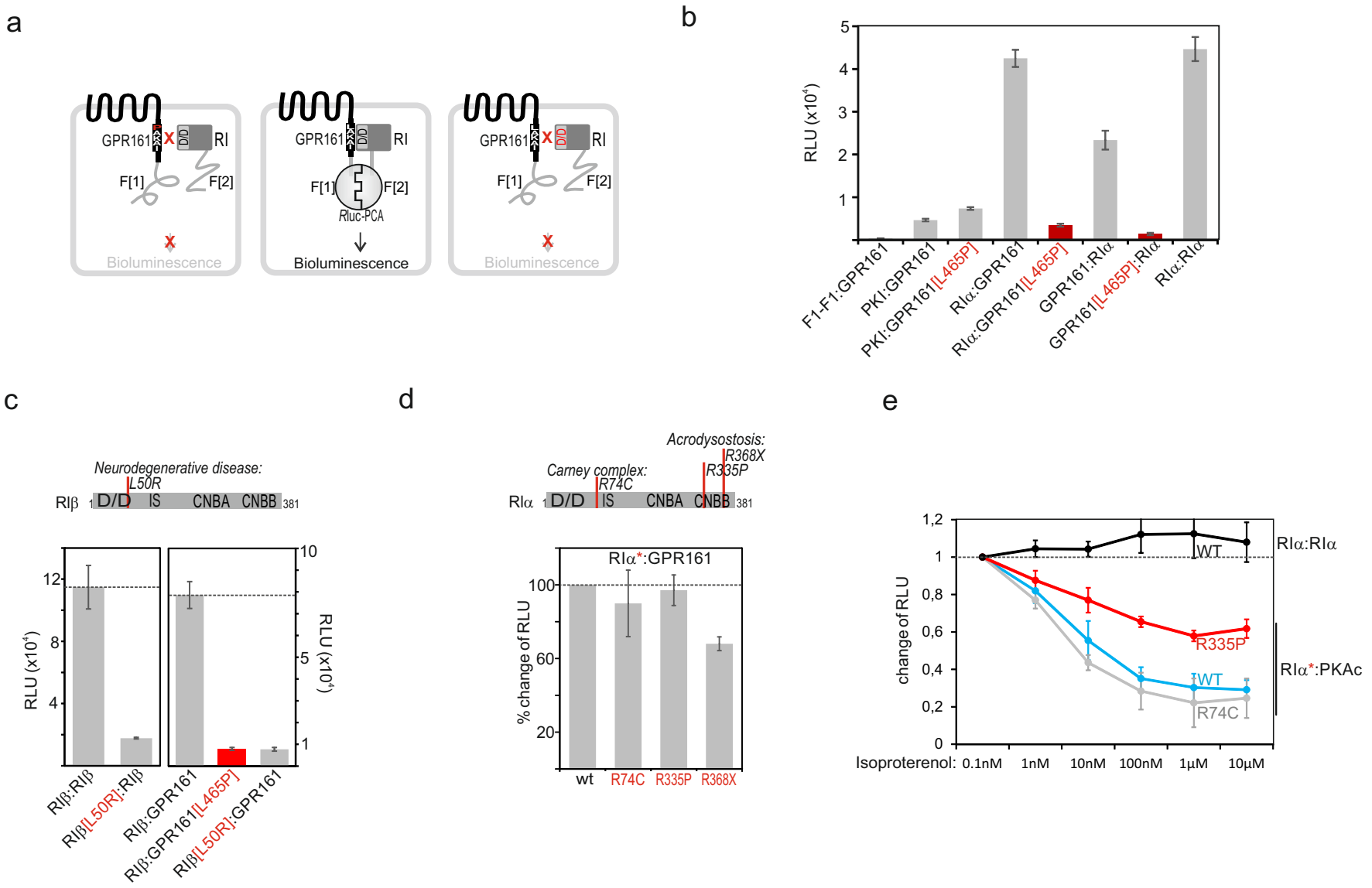
a
GPR161
D/D
RI
F[1]
F[2]
Bioluminescence
Rluc-PCA
b
RLU (x10⁴)
F1-F1:GPR161
PKI:GPR161
PKI:GPR161[L465P]
RIα:GPR161
RIα:GPR161[L465P]
GPR161:RIα
GPR161[L465P]:RIα
RIα:RIα
c
Neurodegenerative disease:
L50R
RIβ
D/D
IS
CNBA
CNBB
RIβ:RIβ
RIβ[L50R]:RIβ
RIβ:GPR161
RIβ:GPR161[L465P]
RIβ[L50R]:GPR161
d
Acrodysostosis:
R368X
Carney complex:
R74C
R335P
RIα
RIα*:GPR161
% change of RLU
wt
R74C
R335P
R368X
e
change of RLU
RIα:RIα
WT
RIα*:PKAc
R335P
WT
R74C
Isoproterenol:
0.1nM
1nM
10nM
100nM
1µM
10µM

Figure 4

Supplementary Figure 1

a

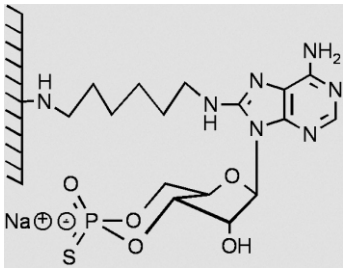

8- (6- Aminohexylamino)adenosine- 3', 5'- cyclic monophosphorothioate, Rp- isomer, immobilized on agarose gel

b

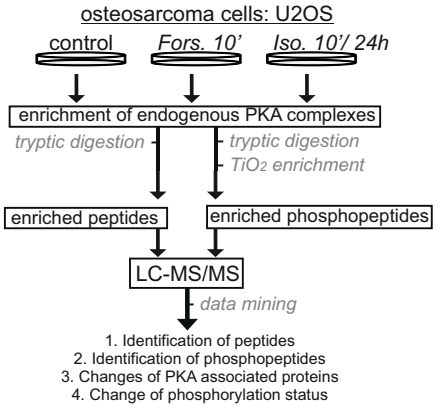

c

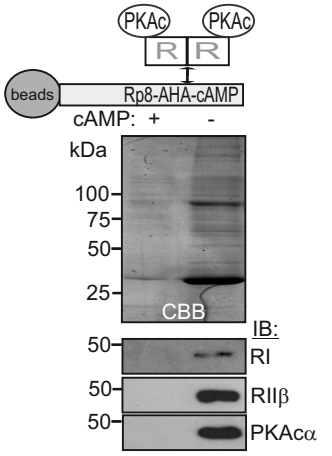

Supplementary Figure 2

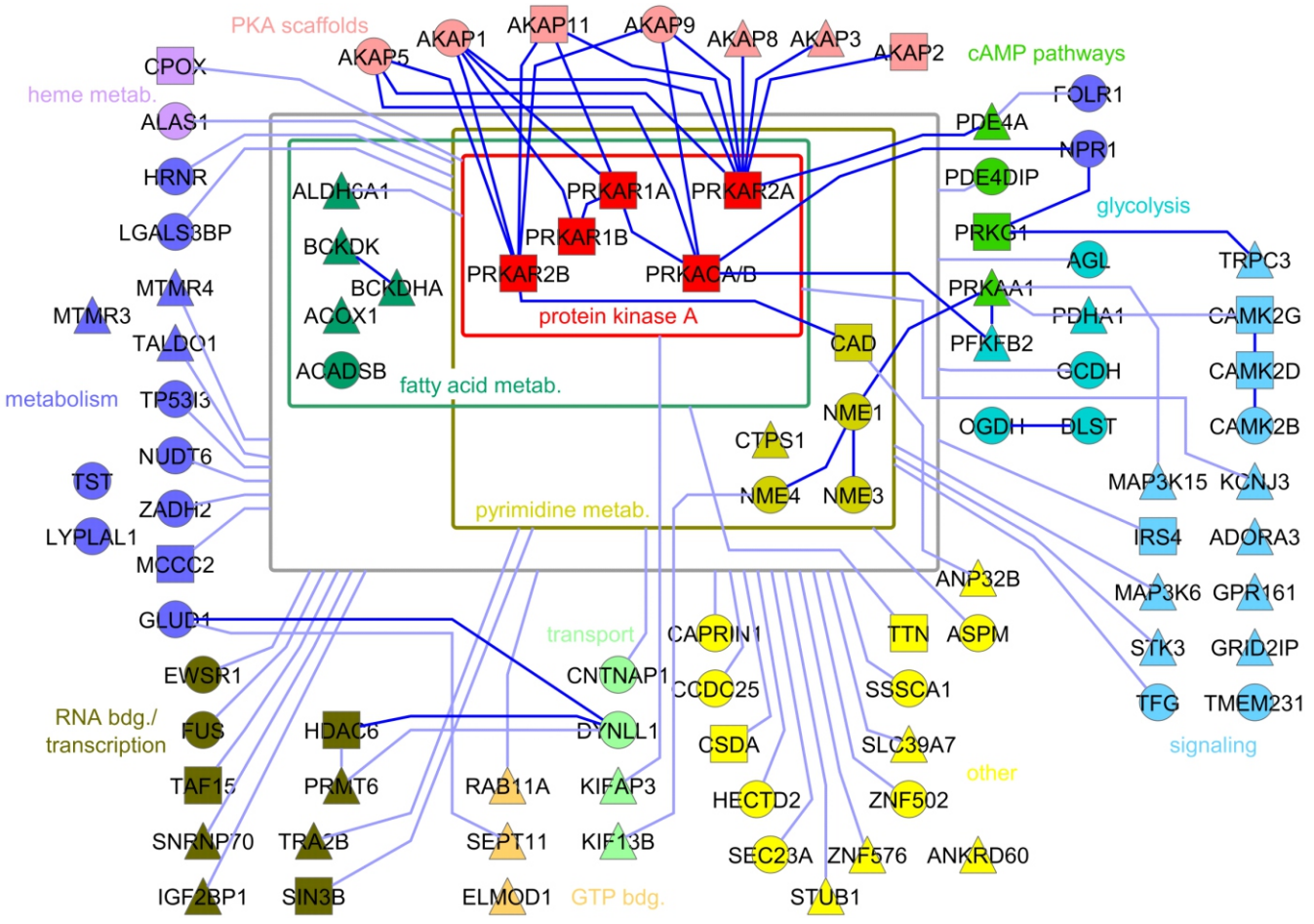

Supplementary Figure 3

a

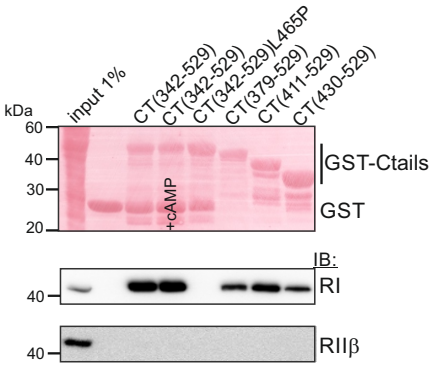

b

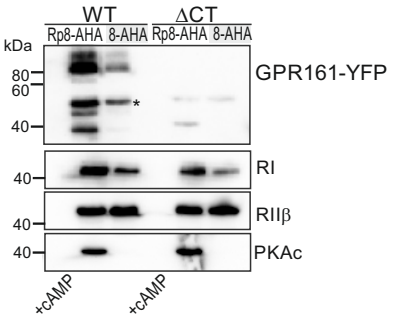

Supplementary Figure 4

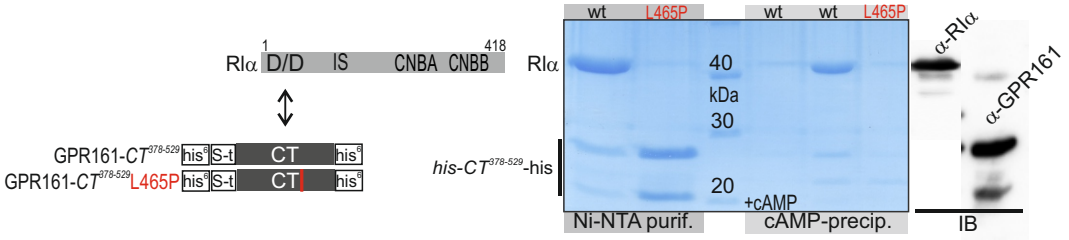

Supplementary Figure 5

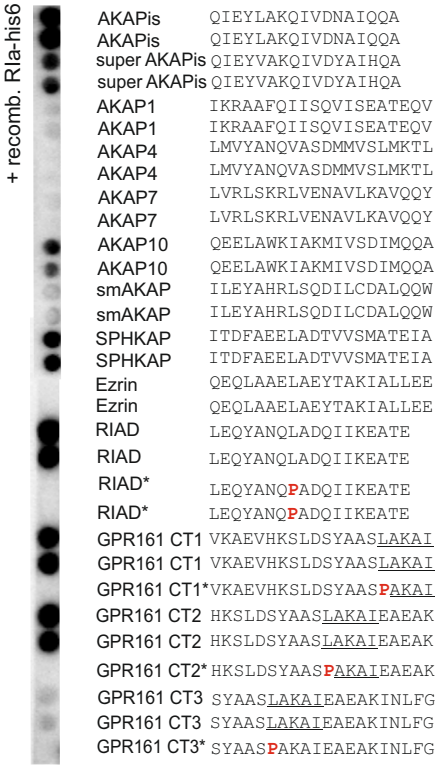

Supplementary Figure 6

a

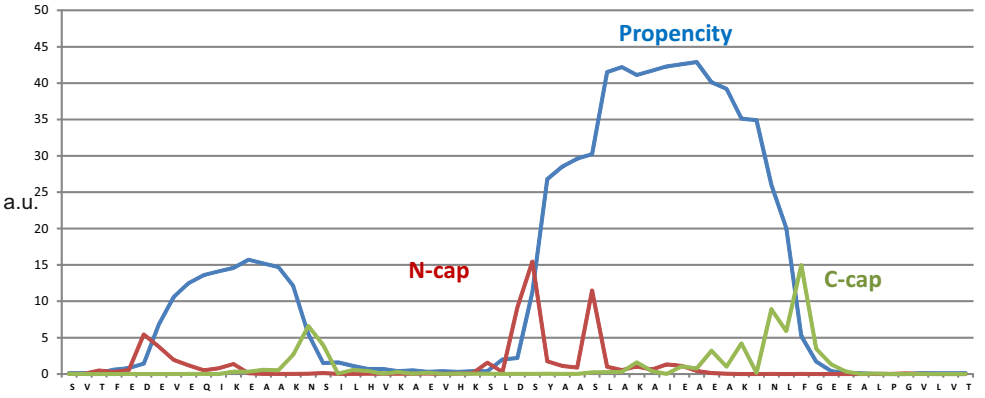

b

RII-specific AKAP

```
28   ELVRLSKRLVENAVLKAV 45   AKAP18
565  TPEEVAAEVLAEVITAAV 582  AKAP95
391  LLIETASSLVKNAIQLSI 408  AKAP79
494  LIEEAASRIVDAVIEQVK 511  Ht31
         : :    :    :
```

Supplementary Figure 7

a

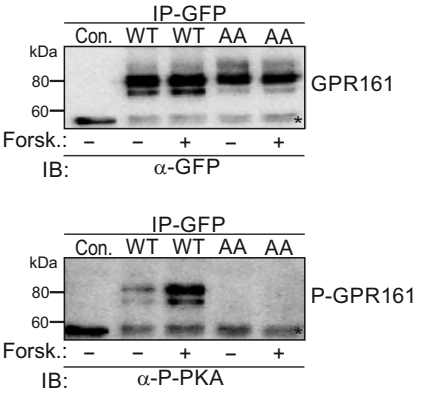

b

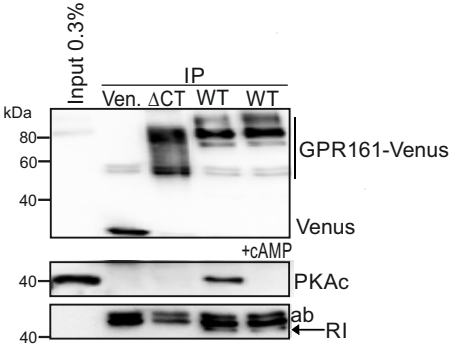

c

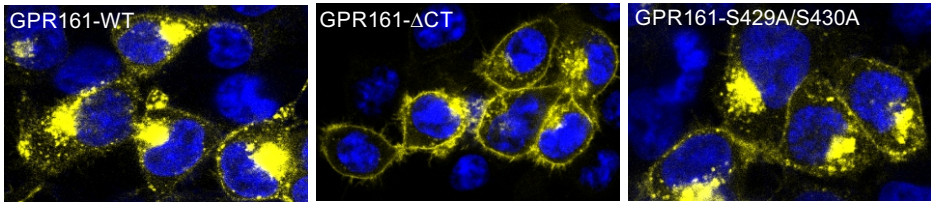

Supplementary Figure 8